Site-specific DNA demethylation during spermatogenesis presets the sites of nucleosome retention in mouse sperm

So Maezawa[1, 2*], Masashi Yukawa[3], Akihiko Sakashita[2, 4], Artem Barski[3], and Satoshi H. Namekawa[2, 5*]

[1] Faculty of Science and Technology, Department of Applied Biological Science, Tokyo University of Science, Chiba 278-8510, Japan.

[2] Division of Reproductive Sciences, Division of Developmental Biology, Perinatal Institute, Cincinnati Children's Hospital Medical Center, Cincinnati, Ohio, 45229, USA

[3] Division of Allergy and immunology, Division of Human Genetics, Cincinnati Children's Hospital Medical Center, Cincinnati, Ohio, 45229, USA

[4] Department of Molecular Biology, Keio University School of Medicine, Tokyo, 160-8582 Japan

[5] Department of Microbiology and Molecular Genetics, University of California Davis, Davis, California, 95616, USA.

* To whom correspondence should be addressed:
So Maezawa, Satoshi H. Namekawa
Email: s-maezawa@tus.ac.jp, snamekawa@ucdavis.edu

Keywords: Germline, Spermatogenesis, Meiosis, DNA methylation, Bivalent domains.

Abstract

DNA methylation patterns are inherited from the parental germline to the embryo. In mature sperm, the sites of unmethylated DNA are tightly coupled to sites of histone retention at gene regulatory elements that are implicated in paternal epigenetic inheritance. The timing and mechanism of site-specific DNA demethylation in the male germline currently remains unknown. Here, we perform genome-wide profiling of DNA methylation during spermatogenesis by capturing methylated DNA through interaction with a methyl-DNA binding protein domain (MBD). Our data demonstrate that there is a site-specific change in DNA methylation during the mitosis-to-meiosis transition. Importantly, the genomic sites that are demethylated during this transition predetermine nucleosome retention sites in spermatozoa. These results suggest that site-specific DNA demethylation during the mitosis-to-meiosis transition of spermatogenesis prepares embryonic gene expression after fertilization. We therefore propose DNA demethylation during spermatogenesis as a novel phase of epigenetic reprogramming that contributes to embryonic gene regulation.

Introduction

Methylation at the 5-carbon position of cytosine (5-methylcytosine: 5mC) at CpG dinucleotides in DNA is dynamically reprogrammed in the parental germline and contributes to epigenetic inheritance from gametes to embryos (Greenberg & Bourc'his, 2019). In mammalian sperm, the vast majority of histones are replaced by protamines, but sites of unmethylated DNA are tightly coupled to sites of histone retention at gene regulatory elements (Erkek et al., 2013). These gene regulatory elements are associated with the embryonic gene expression program after fertilization (Brykczynska et al., 2010; Carone et al., 2014; Erkek et al., 2013; Hammoud et al., 2009; Jung et al., 2019; Jung et al., 2017; Yamaguchi et al., 2018; Yoshida et al., 2018) and therefore contribute to paternal epigenetic inheritance (Gaspa-Toneu & Peters, 2023; Lismer & Kimmins, 2023). However, it remains unknown when specific sites of DNA hypomethylation are established in the male germline to predetermine histone retention sites in spermatozoa.

The sites of histone retention exhibit features of bivalent genomic domains. These domains are characterized by concomitant enrichment of repressive Polycomb Repressive Complex 2 (PRC2)-mediated trimethylation of histone H3 at lysine 27 (H3K27me3) and active di/trimethylation of H3 at lysine 4 (H3K4me2/3) (Brykczynska et al., 2010; Erkek et al., 2013; Hammoud et al., 2014; Hammoud et al., 2009; Lesch et al., 2013; Sachs et al., 2013). Recent studies have demonstrated that alteration of the H3K27me3 and H3K4me3 levels in sperm leads to changes in gene expression in the next generation (Lesch et al., 2019; Lismer et al., 2021; Sakashita et al., 2023; Siklenka et al., 2015).

In the male germline, DNA methylation is largely reprogrammed in primordial germ cells. It globally increases in embryonic prospermatogonia and reaches a level similar to that in spermatozoa in postnatal spermatogonia (~80% of all CpG sites) (Hammoud et al., 2014; Kobayashi et al., 2013; Kubo et al., 2015; Seisenberger et al., 2012). In prospermatogonia, DNA methylation outside of CpG islands, i.e. clusters of CpG dinucleotides that are constitutively hypomethylated, is established through the action of the histone methyltransferase NSD1, the de novo DNA methyltransferase DNMT3A and its catalytically inactive cofactor DNMT3L (Kaneda et al., 2004; Kato et al., 2007; Shirane et al., 2020). Evolutionarily young transposable elements are recognized by the PIWI-interacting RNA (piRNA) pathway and methylated by the germline-

specific de novo DNA methyltransferase DNMT3C (Aravin et al., 2007; Barau et al., 2016; Jain et al., 2017; Kuramochi-Miyagawa et al., 2008).

Based on the studies of paternal genomic imprinting loci, it has long been thought that DNA methylation is stably maintained throughout spermatogenesis following its acquisition in prospermatogonia (Abramowitz & Bartolomei, 2012; Sasaki & Matsui, 2008; Schaefer et al., 2007). Nowadays, mounting evidence suggests a more dynamic nature of DNA methylation during postnatal spermatogenesis. After the postnatal stage, changes in DNA methylation were initially detected in testicular germ cells (Oakes et al., 2007) and during spermatogonial differentiation (Shirakawa et al., 2013). Later studies clarified that, during spermatogenesis, male germ cells undergo a global transient reduction of DNA methylation in early meiotic prophase I (Gaysinskaya et al., 2018; Huang et al., 2023). This process is presumably passive and caused by a delay in establishing maintenance DNA methylation by DNMT1 and its cofactor UHRF1 during premeiotic DNA replication (Gaysinskaya et al., 2018; Huang et al., 2023). Other genome-wide studies have also detected modest changes in DNA methylation during spermatogenesis (Ben Maamar et al., 2022; Chen et al., 2020; Liu et al., 2019; Siebert-Kuss et al., 2024). However, the extent of site-specific regulation of DNA methylation during postnatal spermatogenesis beyond the global transient reduction remains unclear.

To detect site-specific changes in DNA methylation during spermatogenesis, we performed MethylCap-seq during representative stages of spermatogenesis. This approach employs capture of methylated DNA via the Methyl-CpG-binding domain (MBD) followed by next-generation sequencing (Brinkman et al., 2010). Our analysis shows that a site-specific loss of DNA methylation during the mitosis-to-meiosis transition predetermines nucleosome retention sites in mature sperm. Based on these results, we propose that meiosis is a process of epigenetic reprogramming that sets up embryonic gene regulation.

Results

DNA methylation dynamics during spermatogenesis

During mouse spermatogenesis, a transient reduction of DNA methylation occurs globally in the premeiotic S phase. The level of DNA methylation is then gradually recovered in meiotic prophase I (Gaysinskaya et al., 2018; Huang et al., 2023) (Fig. 1A). To evaluate the overall

change before and after this transient reduction of DNA methylation, we first quantified the amount of 5mC during spermatogenesis using an enzyme-linked immunosorbent assay (ELISA). Specifically, we analyzed postnatal day 7 (P7) THY1$^+$ undifferentiated spermatogonia and KIT$^+$ differentiating spermatogonia, both cellular stages prior to the transient reduction. To cover stages of late spermatogenesis after the transient reduction of DNA methylation, we analyzed meiotic pachytene spermatocytes (PS) and postmeiotic rounds spermatids (RS) from adult testes. We found the 5mC level increased during the initial spermatogonial differentiation (Fig. 1B). After the transient reduction, 5mC levels in PS did not recover to the level of KIT$^+$ differentiating spermatogonia, but after meiosis, they slightly increased in RS (Fig. 1B).

To independently evaluate these observations, we performed immunohistochemistry on testicular sections from adult mice. In accordance with the ELISA results, the nuclear 5mC signals increased in differentiating spermatogonia that are devoid of PLZF, a marker of undifferentiated spermatogonia (Fig. 1C). These results are consistent with the earlier observation that 5mC levels increase during spermatogonial differentiation (Shirakawa et al., 2013). In the meiotic prophase, leptotene/zygotene spermatocytes show bright 5mC staining. In contrast, the 5mC signal is diminished in pachytene/diplotene spermatocytes that express the testis-specific histone variant H1T, a maker that is induced after the mid-pachytene stage (Fig. 1D). These results suggest that 5mC levels change dynamically during spermatogenesis before and after the transient reduction of DNA methylation in premeiotic S phase.

Detection of site-specific DNA methylation dynamics in spermatogenesis

Given these dynamic genome-wide methylation changes during spermatogonial differentiation and subsequent meiosis, we sought to determine site-specific 5mC changes. We therefore performed MethylCap-seq (Brinkman et al., 2010), which, unlike whole-genome bisulfite sequencing (WGBS), which does not distinguish between 5mC and 5-hydroxymethylcytosine (5hmC), specifically detects 5mC. While MethylCap-seq does not offer base-pair resolution, it does provide overall profiles of 5mC genome-wide, particularly on dense CpG areas (Nair et al., 2011). In addition, we reasoned that because MethylCap-seq depends on the recognition of 5mC by MBD, the readout of this method represents the recognition by MBD, which may be relevant to functional aspects of 5mC.

We performed MethylCap-seq in wild-type P7 THY^+ and KIT^+ spermatogonia and adult PS and RS with two biological replicates. We detected approximately 130,000 to 200,000 common peaks genome-wide at each transition (Fig. 2A), demonstrating that the overall MethylCap-seq profile largely overlapped between each stage. This observation is in line with the fact that male germ cells acquire global DNA methylation levels similar to spermatozoa before birth. Compared to the number of these common peaks, we detected a relatively small number of unique peaks during spermatogonial differentiation (between THY^+ and KIT^+ spermatogonia) and during the meiosis-to-postmeiosis transition (between PS and RS) (Fig. 2A). In contrast, at the transition from KIT^+ spermatogonia to PS, more site-specific changes in 5mC were detected compared to the other transitions (15,285 KIT^+ unique peaks and 20,934 PS unique peaks). The distribution of these unique peaks encompasses various genomic regions, including intergenic regions, introns, exons, promotes, and upstream regions (Fig. 2A, right panel). A representative track view of a ~ 100kb genomic region in chromosome 17 shows examples of site-specific 5mC gains and losses at the transition between KIT^+ spermatogonia and PS, and these patterns are consistent between biological replicates (Fig. 2B). Average tag density analysis revealed that the loss of 5mC at the KIT^+ to PS transition is pronounced at transcription start sites (TSSs) of late spermatogenesis genes, which are activated at the KIT^+ to PS transition (Sin et al., 2015) (Fig. 2C). Demethylation at TSSs of late spermatogenesis genes, such as *Spata16* and *Slc22a16*, was confirmed both in the MethylCap-seq data and previously-published WGBS data (Hammoud et al., 2014; Kubo et al., 2015) (Fig. S1A). Consistent with this finding, hypomethylation of spermatogenesis genes was recently reported in a human study (Siebert-Kuss et al., 2024). In addition, we observed extensive demethylation at the protocadherin (*Pcdh*) genes of the *Pcdhγ* locus (Fig. S1B). In contrast, 5mC levels did not change extensively in other classes of genes, such as somatic/progenitor genes that are turned off at the KIT^+ to PS transition or genes that are constitutively active or inactive during spermatogenesis (Sin et al., 2015) (Fig. 2C). These results suggest that DNA demethylation at TSSs is associated with activation of late spermatogenesis genes at the KIT^+ to PS transition.

DNA demethylation at TSSs correlates with the activation of late spermatogenesis genes

To further define the changes in the 5mC level at TSSs during spermatogenesis, we compared 5mC levels around all TSSs between two stages through scatter plots of MethylCap-seq read enrichment. Consistent with the peak analysis, 5mC levels around TSSs between THY^+ and KIT^+ spermatogonia and between PS and RS are highly correlated (Fig. 3A). KIT^+ and PS showed a

168 decreased correlation compared to the other transitions (Fig. 3A), although it is still high. These
169 data show overall moderate changes in the 5mC levels between the different cellular stages
170 analyzed. Nevertheless, at the KIT$^+$ to PS transition, 909 TSSs showed a loss of 5mC levels,
171 while 753 TSSs showed a gain of 5mC levels (Fig. 3B).
172
173 In mammals, approximately 70% of genes are linked to promoter CpG islands that are
174 constitutively hypomethylated, while the rest of promoters are depleted in CpGs and subject to
175 context-dependent DNA methylation (Weber et al., 2007). Accordingly, we found that
176 differentially methylated TSSs at the KIT$^+$ to PS transition tend to overlap with low CpG
177 promoters (Fig. 3B, right panel). In this context, TSSs tend to lose rather than gain 5mC levels.
178 GO term analysis revealed that genes that lose 5mC at their TSS are enriched in genes involved in
179 cell adhesion (presumably due to the changes in the *Pcdh* gene cluster seen earlier), sexual
180 reproduction, spermatogenesis, and meiosis (Fig. 3C). This is in line with the demethylation and
181 activation of late spermatogenesis genes described above. On the other hand, genes that show a
182 gain of 5mC are enriched in immune-related functions. This may be related to the fact that the
183 immune system is suppressed (and thus immune-related genes are suppressed) outside of the
184 blood-testis barrier, where spermatogenic differentiation takes place (Cheng & Mruk, 2012).
185
186 We next examined the expression profiles of genes that lose 5mC. This group includes
187 representative late spermatogenesis and meiotic genes, including *Spata16, Tdrd6, Slc22a16,*
188 *Piwil1,* and *Spo11*, which are highly upregulated at the KIT$^+$ to PS transition (Fig. 3D). In
189 contrast, several of the *Pcdh*γ genes show similar expression levels during spermatogenesis (Fig.
190 3D). Further, genes that lose 5mC levels tend to be upregulated at the KIT$^+$ to PS transition
191 compared to genes showing a gain of 5mC levels or all genes (Fig. 3E).
192
193 One special feature of spermatogenic gene expression is a specific expression of single
194 exon genes. Indeed, certain CpG promoters of single exon genes are hypermethylated in soma but
195 hypomethylated in late spermatogenesis (Kato & Nozaki, 2012). We found that, among 2,848
196 single-exon genes, 208 lose 5mC levels at the KIT$^+$ to PS transition (Fig. S2A). 50 of these genes
197 are activated at the KIT$^+$ to PS transition (Fig. S2B). Together, these data suggest that DNA
198 demethylation at TSSs correlates with the activation of late spermatogenesis genes at the KIT$^+$ to
199 PS transition.
200

DNA demethylation during spermatogenesis presets the sites of nucleosome retention in spermatozoa

During spermatogenesis, histones are largely replaced with protamines. In spermatozoa, nucleosomes are retained mainly at hypomethylated TSSs, and these retained nucleosomes are implicated in paternal epigenetic inheritance (Erkek et al., 2013). Since we observed DNA demethylation at a number of TSSs at the KIT^+ to PS transition, we hypothesized that such *de novo* hypomethylated TSSs might serve as the sites of nucleosome retention in spermatozoa. To test this hypothesis, we reanalyzed published MNase-seq data of sperm chromatin (Erkek et al., 2013). Specifically, we examined the degree of nucleosome retention (i.e., the enrichment of mononucleosomes) at various genomic regions detected in our MethylCap-seq data. Interestingly, we found a significant enrichment of mononucleosomes at promoters and exons that lost 5mC at the KIT^+ to PS transition (termed KIT-unique methylated regions) (Fig. 4A). Consistent with these results, nucleosome retention was overserved predominantly at promoters (49%) and exons (18%) in spermatozoa (Fig. 4B).

In spermatozoa, hypomethylated promoters are enriched with histones marked by H3K4me3, which counteracts DNA methylation (Erkek et al., 2013). Thus, we next examined whether promoters and exons that lose 5mC at the KIT^+ to PS transition acquire H3K4me3. We reanalyzed our previous H4K4me3 ChIP-seq data of KIT^+ spermatogonia and PS (Maezawa, Hasegawa, Alavattam, et al., 2018). Our scatter plot analysis shows that at demethylated promoters and exons, there is a gain of H3K4me3 at the KIT^+ to PS transition, and these regions tend to show mononucleosome retention in spermatozoa (Fig. 4C, 4D). These results indicate that during spermatogenesis, DNA demethylation co-occurs with a gain of H3K4-methylation and presets sites of nucleosome retention in sperm.

DNA demethylation leads to nucleosome retention and bivalent chromatin in spermatozoa

Nucleosome retention sites in sperm are implicated in paternal epigenetic inheritance (Erkek et al., 2013). Accumulating evidence suggests incorporation of the histone variant H3.3 and enrichment of bivalent marks, i.e., active H3K4me3 and silent H3K27me3, at these sites (Erkek et al., 2013; Lismer & Kimmins, 2023; Sakashita et al., 2023). Thus, we sought to characterize H3.3 incorporation and bivalent marks of the sites that lose 5mC at the KIT^+ to PS transition in spermatozoa. To this end, we classified the MethylCap-seq peaks of KIT^+ spermatogonia into two classes: peaks which undergo demethylation from KIT^+ spermatogonia to PS (Class I) and all

other peaks (Class II) (Fig. 5A). In spermatozoa, the Class I peaks were enriched in mononucleosomes and H3.3 compared to Class II peaks (Fig. 5A, 5B). Moreover, mononucleosome and H3.3 enrichment in spermatozoa is highly correlated at Class I peaks (Fig. 5C). These results suggest that spermatogenic demethylation precedes the incorporation of histone variant H3.3 and nucleosome retention in spermatozoa.

We next wanted to examine whether bivalent marks are regulated at Class I regions during spermatogenesis. To this end, we focused on germline-specific Polycomb protein SCML2, which has a high affinity to hypomethylated DNA and is a critical regulator of germline transcriptomes and bivalent chromatin (Hasegawa et al., 2015; Maezawa, Hasegawa, Alavattam, et al., 2018; Maezawa et al., 2020; Maezawa, Yukawa, et al., 2018). SCML2 binding sites in spermatogonia predict the sites of H3K27me3 deposition in late spermatogenesis, and loss of SCML2 results in H3K27me3 depletion and defective bivalent domains (Maezawa, Hasegawa, Yukawa, et al., 2018), leading to abnormal paternal epigenetic inheritance (Sakashita et al., 2023). We, therefore, examined the enrichment of SCML2 by reanalyzing our previous SCML2 ChIP-seq data (Hasegawa et al., 2015). The Class I peaks tend to show a higher degree of SCML2 and H3.3 enrichment as well as a higher degree of nucleosome retention than Class II peaks (Fig. 5D). Because SCML2 binds to hypomethylated promoters enriched with H3K4me3 and establishes H3K27me3 in PS (Maezawa, Hasegawa, Alavattam, et al., 2018), we next examined enrichment of H3K4me3 and H3K27me3 at Class I and II peaks during spermatogenesis. In $THY1^+$ and KIT^+ spermatogonia, Class I peaks are enriched with H3K4me3. In contrast, Class II peaks are not enriched with H3K4me3 (Fig. 5E). The Class I peaks gradually gain H3K27me3 during the differentiation from PS to spermatozoa and the majority of Class I peaks are enriched with both H3K4me3 and H3K27me3 in spermatozoa (Fig. 5E). Taken together, we conclude that spermatogenic demethylation precedes nucleosome retention enriched with bivalent marks H3K4me3 and H3K27me3 in spermatozoa.

Finally, we investigated how spermatogenic demethylation affects gene expression in embryos. Genes whose promoters are enriched with nucleosomes in spermatozoa (top 1,000 nucleosome-enriched genes among class I and II peak-containing genes at promoters) are highly expressed in embryogenesis at 2-cell and 4-cell stages and at embryonic day 10.5 (E10.5) (Fig. 5F), although we did not observe an apparent difference between these two groups. This is highly significant when compared to genes whose promoters are depleted with nucleosomes (bottom

3000 nucleosome-enriched genes) in spermatozoa. Thus, nucleosome enrichment in spermatozoa is associated with gene expression in early embryos. These results suggest that the genes that undergo spermatogenic demethylation are enriched with nucleosomes in spermatozoa and are expressed in embryos of the next generation.

Discussion

In this study, we have mapped site-specific DNA methylation during the transition from mitotic spermatogonia to meiotic spermatocytes. We observed that promoters of a large number of late spermatogenesis genes undergo DNA demethylation at the KIT^{+} spermatogonia to PS transition, indicating that DNA demethylation might mark late spermatogenesis genes for induction. Our data also suggest that these demethylated regions predetermine sites of nucleosome retention in spermatozoa. Specifically, we propose that demethylated regions in meiotic spermatocytes acquire H3K4me3 and induce SCML2-mediated deposition of H3K27me3, thereby establishing bivalent marks at these hypomethylated nucleosome retention sites in spermatozoa (Fig. 6). In support of this model, we recently demonstrated that SCML2 mediates paternal epigenetic inherence through sperm chromatin (Sakashita et al., 2023).

Our data revealed a novel feature of the male germline in which site-specific DNA demethylation during postnatal spermatogenesis, specifically in meiosis, provides heritable information from sperm to embryos. Based on these data, we propose that meiosis is an epigenetic reprogramming process that sets up embryonic gene regulation. In 1984, Robin Holliday proposed that an aspect of the biological significance of meiosis is the reprogramming of gametes for fertilization (Holliday, 1984), and our data provide a foundation for this concept.

The site-specific regulation of DNA methylation described in this study is distinct from the transient reduction of DNA methylation that occurs in the premeiotic S phase (Gaysinskaya et al., 2018; Huang et al., 2023). This transient reduction appears to be a passive process due to delays in the establishment of maintenance DNA methylation. Therefore, it is global and not site-specific. Furthermore, the DNA remains hemimethylated. The site-specific regulation that we observe here might be an active process mediated by TET enzymes during the post-mitotic stage. In support of this possibility, TET enzymes were required in the germline (Dawlaty et al., 2013). Furthermore, a recent study demonstrated that TET1 is required for the patterning of

hypomethylated regions in mouse spermatozoa (Prasasya et al., 2024). Alternatively, it could be caused by protection from maintenance DNA methylation and subsequent prevention of de novo DNA methylation during mitotic proliferation of spermatogonia. Further determination of the DNA demethylation mechanism in spermatogenesis is required in future studies. In addition to DNA demethylation mechanisms, a possible function of de novo DNA methyltransferases in modulating nucleosome retention in sperm was recently suggested (Fanourgakis et al., 2024). Thus, it is conceivable that DNA demethylation mechanisms and DNA methyltransferase activities are intricately regulated to shape DNA methylation profiles in spermatozoa.

The paternal genome undergoes extensive reprogramming after fertilization. For example, paternal H3.3 on promoters disappears after fertilization (Ishiuchi et al., 2021), H3K27me3 is reprogrammed during preimplantation development (Zheng et al., 2016) and the paternal genome undergoes passive and active DNA demethylation (Guo et al., 2014; Shen et al., 2014; Wang et al., 2014). Thus, a major unsolved mystery is how paternal epigenetic states are inherited and maintained after fertilization. One possibility is that the paternal epigenetic states, reflecting the memory of paternal hypomethylated DNA, escape epigenetic reprogramming and persist at the promoter regions of the target genes throughout germ cell development. Nevertheless, this possibility has been confounded by the debates about the sites of nucleosome retention in spermatozoa (Yin et al., 2023). Therefore, an important next step is to elucidate how the paternal hypomethylated DNA regions are regulated in the sperm-to-zygote transition.

Materials and Methods

Animals

Mice on the C57BL/6 background were maintained and used according to the guidelines of the Institutional Animal Care and Use Committee (protocol no. IACUC2018–0040) at Cincinnati Children's Hospital Medical Center.

Germ cell fractionation

Wild-type mice on the C57BL/6 background (at least 12 independent mice at 8-12 weeks of age or at least 20 independent mice at 6-8 days of age) were used for isolation of germ cells. Pachytene spermatocytes and round spermatids were isolated via BSA gravity sedimentation as previously described (Bellve, 1993). Purity was confirmed by nuclear staining with Hoechst

33342 using fluorescence microscopy. In keeping with previous studies from the Namekawa lab (Alavattam et al., 2019; Hasegawa et al., 2015; Maezawa, Hasegawa, Yukawa, et al., 2018; Maezawa, Yukawa, et al., 2018), only fractions with a mean purity of ≥90% were used to extract genomic DNA.

Spermatogonia were isolated as described previously (Hammoud et al., 2014) and collected from C57BL/6 wild-type mice aged 6–8 days. Testes were collected in a 24-well plate in Dulbecco's Modified Eagle Medium (DMEM) supplemented with GlutaMax (Thermo Fisher Scientific), non-essential amino acids (NEAA) (Thermo Fisher Scientific), and penicillin and streptomycin (Thermo Fisher Scientific). After removing the *tunica albuginea* membrane, testes were digested with collagenase (1 mg/ml) at 34°C for 20 min to remove interstitial cells, then centrifuged at 188×*g* for 5 min. Tubules were washed with the medium and then digested with trypsin (2.5 mg/ml) at 34°C for 20 min to obtain a single-cell suspension. Cells were filtered with a 40-μm strainer to remove Sertoli cells, and the cell suspension was plated in a 24-well plate for 1 h in the medium supplemented with 10% fetal bovine serum, which promotes adhesion of remaining somatic cells. Cells were washed with magnetic cell-sorting (MACS) buffer (PBS supplemented with 0.5% BSA and 5 mM EDTA) and incubated with CD117 (KIT) MicroBeads (Miltenyi Biotec) on ice for 20 min. Cells were washed and resuspended with MACS buffer and filtered with a 40-μm strainer. Cells were separated by autoMACS Pro Separator (Miltenyi Biotec) with the program "possel." Cells in the flow-through fraction were washed with MACS buffer and incubated with CD90.2 (THY1) MicroBeads (Miltenyi Biotec) on ice for 20 min. Cells were washed and resuspended with MACS buffer and filtered with a 40-μm strainer. Cells were separated by autoMACS Pro Separator (Miltenyi Biotec) with the program "posseld." Purity was confirmed by immunostaining.

Quantification of 5mC

Genomic DNA was purified from isolated germ cells using Genomic DNA Clean & Concentrator Kit (ZynoResearch) according to the manual provided. The percentage of 5mC in total DNA was quantified by MethylFlash™ Methylated 5mC DNA Quantification Kit (Colorimetric) (Epigentek) according to the manual provided.

Histological analysis and immunofluorescence

For the preparation of testicular paraffin blocks, testes were fixed with 4% paraformaldehyde (PFA) overnight at 4°C with gentle inverting. Testes were dehydrated and embedded in paraffin. For immunofluorescence analysis of testicular sections, antigen retrieval was performed by boiling the slides in Target Retrieval Solution (DAKO) for 10 min and letting the solution cool for 30 min. For the detection of 5mC, sections were incubated in 4 N HCl for 1 h at room temperature and then neutralized in 100 mM Tris-HCl (pH 8.5) for 10 min, followed by a standard immunostaining protocol. Sections were blocked with Blocking One Histo (Nacalai) for 1 h at room temperature and then incubated with anti-5mC (1/200 dilution, Eurogentec, clone 33D3), anti-ZBTB16 (1/200 dilution, Santa Cruz, sc22839), and anti-H1T (1/1000 dilution, gift from Dr. Mary Ann Handel) antibodies overnight at 4°C. The resulting signals were detected by incubation with secondary antibodies conjugated to Alexa Fluor dyes (Thermo Fisher Scientific or Jackson ImmunoResearch). Sections were counterstained with DAPI. Images were obtained via a laser scanning confocal microscope A1R (Nikon) and processed with NIS-Elements (Nikon) and ImageJ (National Institutes of Health) (Schneider et al., 2012).

MethylCap-seq

Genomic DNA was fragmentated by sonication and methylated DNA fragments were captured by MethylAffinity Methylated DNA Enrichment Kit (GeneCopoeia). DNA libraries were created by ChIPmentation method (Schmidl et al., 2015). Briefly, methylated DNA fragment-bound beads were resuspended in 30 µl of the tagmentation reaction buffer (10 mM Tris-HCl pH 8.0 and 5 mM $MgCl_2$) containing 1 µl Tagment DNA Enzyme from the Nextera DNA Sample Prep Kit (Illumina) and incubated at 37°C for 10 min in a thermal cycler. The beads were washed twice with 150 µl cold wash buffer (50 mM Tris-HCl pH 8.0, 150 mM NaCl, 1 mM EDTA, 0.1% SDS, 0.1% NaDOC, and 1% Triton X-100), incubated with elution buffer (10 mM Tris-HCl pH 8.0, 1 mM EDTA, 250 mM NaCl, 0.3% SDS, 0.1 µg/µl Proteinase K) at 42°C for 30 min. DNA was purified with the MinElute Reaction Cleanup Kit (Qiagen) and amplified with NEBNext High-Fidelity 2× PCR Master Mix (NEB). Amplified DNA was purified by Agencourt AMPure XP (Beckman Coulter). Afterward, DNA fragments in the 250- to 500-bp size range were prepared by agarose gel size selection. DNA libraries were adjusted to 5 nM in 10 mM Tris-HCl pH 8.0 and sequenced with an Illumina HiSeq 2500.

Data analysis

Data analysis for MethylCap-seq, ChIP-seq, and RNA-seq was performed in the BioWardrobe Experiment Management System (Kartashov & Barski, 2015). For MethylCap-seq and ChIP-seq analysis, reads were aligned to mouse genome mm10 with Bowtie (version 1.2.0, (Langmead et al., 2009)), assigned to NCBI RefSeq genes or isoforms, and coverage was displayed on a local mirror of the UCSC genome browser (Meyer et al., 2013). MethylCap-seq peaks were identified using MACS2 (version 2.1.1.20160309, (Zhang et al., 2008)) with a default parameter setting for narrow peak detection in BioWardrobe. Pearson correlations for the genome-wide enrichment of the peaks among MethylCap-seq library replicates were analyzed using SeqMonk (Babraham Institute).

MAnorm, software designed for quantitative comparisons of ChIP-seq data sets (Shao et al., 2012), was used to compare the genome-wide MethylCap-seq peaks among stages in spermatogenesis. Unique peaks were defined using the following criteria: (1) defined as “unique” by the MAnorm algorithm; (2) P-value <0.01; (3) raw counts of unique reads >10. Peaks common to two stages were defined using the following criteria: (1) defined as “common” by MAnorm algorithm; (2) raw read counts of both stages >10.

Average tag density profiles were calculated around transcription start sites for gene sets of somatic/progenitor genes, late spermatogenesis genes, constitutive active genes, and constitutive inactive genes, as described previously (Sin et al., 2015). The resulting graphs were smoothed in 200-bp windows. Enrichment levels for MethylCap-seq experiments were calculated for 10-kb windows, promoter regions of genes (±5 kb surrounding TSSs).

Enrichment levels for MethylCap-seq and ChIP-seq experiments were calculated for 4-kb windows, promoter regions of genes (±2 kb surrounding TSSs). To normalize tag values, read counts were multiplied by 1,000,000 and then divided by the total number of reads in each nucleotide position. The total amount of tag values in promoter or enhancer regions was calculated as enrichment.

To detect differentially methylated regions around TSSs among stages in spermatogenesis, a read count output file was input to the DESeq2 package (version 1.16.1); then, the program functions DESeqDataSetFromMatrix and DESeq were used to compare each gene’s expression level between two biological samples. Differentially methylated regions were identified through

binominal tests, thresholding Benjamini-Hochberg- adjusted P values to <0.05. To perform gene ontology analyses, the functional annotation clustering tool in DAVID (version 6.8) was used, and a background of all mouse genes was applied.

For RNA-seq analysis, reads were aligned by STAR (version STAR_2.5.3a) (Dobin et al., 2013)) (Dobin et al., 2013) with default arguments except --outFilterMultimapNmax 1 and --outFilterMismatchNmax 2. The --outFilterMultimapNmax parameter was used to allow unique alignments only, and the --outFilterMismatchNmax parameter was used to allow a maximum of 2 errors. NCBI RefSeq annotation from the mm10 UCSC genome browser was used, and canonical TSSs (1 TSS per gene) were analyzed. All reads from the resulting .bam files were split for related isoforms with respect to RefSeq annotation.

Data availability

NGS datasets used in this study are publicly available and referenced within the article. All the MethylCap-seq data generated in this study are deposited to the Gene Expression Omnibus (GEO) under accession code GSE262669.

Author Contributions

S.M. and S.H.N. designed research; S.M. performed research; S.M., M. Y., A.S. A.B., and S.H.N. analyzed data; and S.M. and S.H.N. wrote the paper. S.H.N. supervised the project.

Acknowledgments

We thank members of the Namekawa and Maezawa labs for discussion and helpful comments regarding the manuscript.

Funding

JSPS KAKENHI Grant Numbers 23H04292, 23K18084, 23H04950, the Takeda Science Foundation, Astellas Foundation for Research on Metabolic Disorders, and TERUMO LIFE SCIENCE FOUNDATION to SM to S.M., and NIH Grants GM119134 to A.B., GM122776 and GM141085 to S.H.N.

Conflict of interest statements

AB is a co-founder of Datirium, LLC.

References

Abramowitz, L. K., & Bartolomei, M. S. (2012). Genomic imprinting: recognition and marking of imprinted loci. *Curr Opin Genet Dev*, *22*(2), 72-78. https://doi.org/10.1016/j.gde.2011.12.001

Alavattam, K. G., Maezawa, S., Sakashita, A., Khoury, H., Barski, A., Kaplan, N., & Namekawa, S. H. (2019). Attenuated chromatin compartmentalization in meiosis and its maturation in sperm development. *Nat Struct Mol Biol*, *26*(3), 175-184. https://doi.org/10.1038/s41594-019-0189-y

Aravin, A. A., Sachidanandam, R., Girard, A., Fejes-Toth, K., & Hannon, G. J. (2007). Developmentally regulated piRNA clusters implicate MILI in transposon control. *Science*, *316*(5825), 744-747. https://doi.org/10.1126/science.1142612

Barau, J., Teissandier, A., Zamudio, N., Roy, S., Nalesso, V., Hérault, Y., Guillou, F., & Bourc'his, D. (2016). The DNA methyltransferase DNMT3C protects male germ cells from transposon activity. *Science*, *354*(6314), 909-912. https://doi.org/10.1126/science.aah5143

Bellve, A. R. (1993). Purification, culture, and fractionation of spermatogenic cells. *Methods Enzymol*, *225*, 84-113. http://www.ncbi.nlm.nih.gov/pubmed/8231890

Ben Maamar, M., Beck, D., Nilsson, E., McCarrey, J. R., & Skinner, M. K. (2022). Developmental alterations in DNA methylation during gametogenesis from primordial germ cells to sperm. *iScience*, *25*(2), 103786. https://doi.org/10.1016/j.isci.2022.103786

Brinkman, A. B., Simmer, F., Ma, K., Kaan, A., Zhu, J., & Stunnenberg, H. G. (2010). Whole-genome DNA methylation profiling using MethylCap-seq. *Methods*, *52*(3), 232-236. https://doi.org/10.1016/j.ymeth.2010.06.012

Brykczynska, U., Hisano, M., Erkek, S., Ramos, L., Oakeley, E. J., Roloff, T. C., Beisel, C., Schubeler, D., Stadler, M. B., & Peters, A. H. (2010). Repressive and active histone methylation mark distinct promoters in human and mouse spermatozoa. *Nat Struct Mol Biol*, *17*(6), 679-687. https://doi.org/10.1038/nsmb.1821

Carone, B. R., Hung, J. H., Hainer, S. J., Chou, M. T., Carone, D. M., Weng, Z., Fazzio, T. G., & Rando, O. J. (2014). High-resolution mapping of chromatin packaging in mouse embryonic stem cells and sperm. *Dev Cell*, *30*(1), 11-22. https://doi.org/10.1016/j.devcel.2014.05.024

Chen, Y., Lyu, R., Rong, B., Zheng, Y., Lin, Z., Dai, R., Zhang, X., Xie, N., Wang, S., Tang, F., Lan, F., & Tong, M. H. (2020). Refined spatial temporal epigenomic profiling reveals intrinsic connection between PRDM9-mediated H3K4me3 and the fate of double-stranded breaks. *Cell Res*, *30*(3), 256-268. https://doi.org/10.1038/s41422-020-0281-1

Cheng, C. Y., & Mruk, D. D. (2012). The blood-testis barrier and its implications for male contraception. *Pharmacol Rev*, *64*(1), 16-64. https://doi.org/10.1124/pr.110.002790

Dawlaty, M. M., Breiling, A., Le, T., Raddatz, G., Barrasa, M. I., Cheng, A. W., Gao, Q., Powell, B. E., Li, Z., Xu, M., Faull, K. F., Lyko, F., & Jaenisch, R. (2013). Combined deficiency of Tet1 and Tet2 causes epigenetic abnormalities but is compatible with postnatal development. *Dev Cell*, *24*(3), 310-323. https://doi.org/10.1016/j.devcel.2012.12.015

Dobin, A., Davis, C. A., Schlesinger, F., Drenkow, J., Zaleski, C., Jha, S., Batut, P., Chaisson, M., & Gingeras, T. R. (2013). STAR: ultrafast universal RNA-seq aligner. *Bioinformatics*, *29*(1), 15-21. https://doi.org/10.1093/bioinformatics/bts635

Erkek, S., Hisano, M., Liang, C. Y., Gill, M., Murr, R., Dieker, J., Schübeler, D., van der Vlag, J., Stadler, M. B., & Peters, A. H. (2013). Molecular determinants of nucleosome retention at CpG-rich sequences in mouse spermatozoa. *Nat Struct Mol Biol*, *20*(7), 868-875. https://doi.org/10.1038/nsmb.2599

Fanourgakis, G., Gaspa-Toneu, L., Komarov, P. A., Ozonov, E. A., Smallwood, S. A., & Peters, A. H. F. M. (2024). DNA methylation modulates nucleosome retention in sperm and H3K4 methylation deposition in early mouse embryos. *bioRxiv*, 2024.2002.2006.579069. https://doi.org/10.1101/2024.02.06.579069

Gaspa-Toneu, L., & Peters, A. H. (2023). Nucleosomes in mammalian sperm: conveying paternal epigenetic inheritance or subject to reprogramming between generations? *Curr Opin Genet Dev*, *79*, 102034. https://doi.org/10.1016/j.gde.2023.102034

Gaysinskaya, V., Miller, B. F., De Luca, C., van der Heijden, G. W., Hansen, K. D., & Bortvin, A. (2018). Transient reduction of DNA methylation at the onset of meiosis in male mice. *Epigenetics Chromatin*, *11*(1), 15. https://doi.org/10.1186/s13072-018-0186-0

Greenberg, M. V. C., & Bourc'his, D. (2019). The diverse roles of DNA methylation in mammalian development and disease. *Nat Rev Mol Cell Biol*, *20*(10), 590-607. https://doi.org/10.1038/s41580-019-0159-6

Guo, F., Li, X., Liang, D., Li, T., Zhu, P., Guo, H., Wu, X., Wen, L., Gu, T. P., Hu, B., Walsh, C. P., Li, J., Tang, F., & Xu, G. L. (2014). Active and passive demethylation of male and female pronuclear DNA in the mammalian zygote. *Cell Stem Cell*, *15*(4), 447-459. https://doi.org/10.1016/j.stem.2014.08.003

Hammoud, S. S., Low, D. H., Yi, C., Carrell, D. T., Guccione, E., & Cairns, B. R. (2014). Chromatin and transcription transitions of mammalian adult germline stem cells and spermatogenesis. *Cell Stem Cell*, *15*(2), 239-253. https://doi.org/10.1016/j.stem.2014.04.006

Hammoud, S. S., Nix, D. A., Zhang, H., Purwar, J., Carrell, D. T., & Cairns, B. R. (2009). Distinctive chromatin in human sperm packages genes for embryo development. *Nature*, *460*(7254), 473-478. https://doi.org/10.1038/nature08162

Hasegawa, K., Sin, H. S., Maezawa, S., Broering, T. J., Kartashov, A. V., Alavattam, K. G., Ichijima, Y., Zhang, F., Bacon, W. C., Greis, K. D., Andreassen, P. R., Barski, A., & Namekawa, S. H. (2015). SCML2 establishes the male germline epigenome through regulation of histone H2A ubiquitination. *Dev Cell*, *32*(5), 574-588. https://doi.org/10.1016/j.devcel.2015.01.014

Holliday, R. (1984). The biological significance of meiosis. *Symp Soc Exp Biol*, *38*, 381-394.

Huang, Y., Li, L., An, G., Yang, X., Cui, M., Song, X., Lin, J., Zhang, X., Yao, Z., Wan, C., Zhou, C., Zhao, J., Song, K., Ren, S., Xia, X., Fu, X., Lan, Y., Hu, X., Wang, W., . . . Zhao, X. Y. (2023). Single-cell multi-omics sequencing of human spermatogenesis reveals a DNA demethylation event associated with male meiotic recombination. *Nat Cell Biol*, *25*(10), 1520-1534. https://doi.org/10.1038/s41556-023-01232-7

Ishiuchi, T., Abe, S., Inoue, K., Yeung, W. K. A., Miki, Y., Ogura, A., & Sasaki, H. (2021). Reprogramming of the histone H3.3 landscape in the early mouse embryo. *Nat Struct Mol Biol*, *28*(1), 38-49. https://doi.org/10.1038/s41594-020-00521-1

Jain, D., Meydan, C., Lange, J., Claeys Bouuaert, C., Lailler, N., Mason, C. E., Anderson, K. V., & Keeney, S. (2017). rahu is a mutant allele of Dnmt3c, encoding a DNA methyltransferase homolog required for meiosis and transposon repression in the mouse male germline. *PLoS Genet*, *13*(8), e1006964. https://doi.org/10.1371/journal.pgen.1006964

Jung, Y. H., Kremsky, I., Gold, H. B., Rowley, M. J., Punyawai, K., Buonanotte, A., Lyu, X., Bixler, B. J., Chan, A. W. S., & Corces, V. G. (2019). Maintenance of CTCF- and Transcription Factor-Mediated Interactions from the Gametes to the Early Mouse Embryo. *Mol Cell*, *75*(1), 154-171.e155. https://doi.org/10.1016/j.molcel.2019.04.014

Jung, Y. H., Sauria, M. E. G., Lyu, X., Cheema, M. S., Ausio, J., Taylor, J., & Corces, V. G. (2017). Chromatin States in Mouse Sperm Correlate with Embryonic and Adult

Regulatory Landscapes. *Cell Rep*, *18*(6), 1366-1382. https://doi.org/10.1016/j.celrep.2017.01.034

Kaneda, M., Okano, M., Hata, K., Sado, T., Tsujimoto, N., Li, E., & Sasaki, H. (2004). Essential role for de novo DNA methyltransferase Dnmt3a in paternal and maternal imprinting. *Nature*, *429*(6994), 900-903. https://doi.org/10.1038/nature02633

Kartashov, A. V., & Barski, A. (2015). BioWardrobe: an integrated platform for analysis of epigenomics and transcriptomics data. *Genome Biol*, *16*(1), 158. https://doi.org/10.1186/s13059-015-0720-3

Kato, Y., Kaneda, M., Hata, K., Kumaki, K., Hisano, M., Kohara, Y., Okano, M., Li, E., Nozaki, M., & Sasaki, H. (2007). Role of the Dnmt3 family in de novo methylation of imprinted and repetitive sequences during male germ cell development in the mouse. *Hum Mol Genet*, *16*(19), 2272-2280. https://doi.org/10.1093/hmg/ddm179

Kato, Y., & Nozaki, M. (2012). Distinct DNA methylation dynamics of spermatogenic cell-specific intronless genes is associated with CpG content. *PLoS One*, *7*(8), e43658. https://doi.org/10.1371/journal.pone.0043658

Kobayashi, H., Sakurai, T., Miura, F., Imai, M., Mochiduki, K., Yanagisawa, E., Sakashita, A., Wakai, T., Suzuki, Y., Ito, T., Matsui, Y., & Kono, T. (2013). High-resolution DNA methylome analysis of primordial germ cells identifies gender-specific reprogramming in mice. *Genome Res*, *23*(4), 616-627. https://doi.org/10.1101/gr.148023.112

Kubo, N., Toh, H., Shirane, K., Shirakawa, T., Kobayashi, H., Sato, T., Sone, H., Sato, Y., Tomizawa, S., Tsurusaki, Y., Shibata, H., Saitsu, H., Suzuki, Y., Matsumoto, N., Suyama, M., Kono, T., Ohbo, K., & Sasaki, H. (2015). DNA methylation and gene expression dynamics during spermatogonial stem cell differentiation in the early postnatal mouse testis. *BMC Genomics*, *16*(1), 624. https://doi.org/10.1186/s12864-015-1833-5

Kuramochi-Miyagawa, S., Watanabe, T., Gotoh, K., Totoki, Y., Toyoda, A., Ikawa, M., Asada, N., Kojima, K., Yamaguchi, Y., Ijiri, T. W., Hata, K., Li, E., Matsuda, Y., Kimura, T., Okabe, M., Sakaki, Y., Sasaki, H., & Nakano, T. (2008). DNA methylation of retrotransposon genes is regulated by Piwi family members MILI and MIWI2 in murine fetal testes. *Genes Dev*, *22*(7), 908-917. https://doi.org/10.1101/gad.1640708

Langmead, B., Trapnell, C., Pop, M., & Salzberg, S. L. (2009). Ultrafast and memory-efficient alignment of short DNA sequences to the human genome. *Genome Biol*, *10*(3), R25. https://doi.org/10.1186/gb-2009-10-3-r25

Lesch, B. J., Dokshin, G. A., Young, R. A., McCarrey, J. R., & Page, D. C. (2013). A set of genes critical to development is epigenetically poised in mouse germ cells from fetal stages through completion of meiosis. *Proc Natl Acad Sci U S A*, *110*(40), 16061-16066. https://doi.org/10.1073/pnas.1315204110

Lesch, B. J., Tothova, Z., Morgan, E. A., Liao, Z., Bronson, R. T., Ebert, B. L., & Page, D. C. (2019). Intergenerational epigenetic inheritance of cancer susceptibility in mammals. *Elife*, *8*. https://doi.org/10.7554/eLife.39380

Lismer, A., Dumeaux, V., Lafleur, C., Lambrot, R., Brind'Amour, J., Lorincz, M. C., & Kimmins, S. (2021). Histone H3 lysine 4 trimethylation in sperm is transmitted to the embryo and associated with diet-induced phenotypes in the offspring. *Dev Cell*, *56*(5), 671-686.e676. https://doi.org/10.1016/j.devcel.2021.01.014

Lismer, A., & Kimmins, S. (2023). Emerging evidence that the mammalian sperm epigenome serves as a template for embryo development. *Nat Commun*, *14*(1), 2142. https://doi.org/10.1038/s41467-023-37820-2

Liu, Y., Zhang, Y., Yin, J., Gao, Y., Li, Y., Bai, D., He, W., Li, X., Zhang, P., Li, R., Zhang, L., Jia, Y., Zhang, Y., Lin, J., Zheng, Y., Wang, H., Gao, S., Zeng, W., & Liu, W. (2019). Distinct H3K9me3 and DNA methylation modifications during mouse spermatogenesis. *J Biol Chem*, *294*(49), 18714-18725. https://doi.org/10.1074/jbc.RA119.010496

610 Maezawa, S., Hasegawa, K., Alavattam, K. G., Funakoshi, M., Sato, T., Barski, A., & Namekawa,
611 S. H. (2018). SCML2 promotes heterochromatin organization in late spermatogenesis. *J*
612 *Cell Sci*, *131*(17). https://doi.org/10.1242/jcs.217125
613 Maezawa, S., Hasegawa, K., Yukawa, M., Kubo, N., Sakashita, A., Alavattam, K. G., Sin, H. S.,
614 Kartashov, A. V., Sasaki, H., Barski, A., & Namekawa, S. H. (2018). Polycomb protein
615 SCML2 facilitates H3K27me3 to establish bivalent domains in the male germline. *Proc*
616 *Natl Acad Sci U S A*, *115*(19), 4957-4962. https://doi.org/10.1073/pnas.1804512115
617 Maezawa, S., Sakashita, A., Yukawa, M., Chen, X., Takahashi, K., Alavattam, K. G., Nakata, I.,
618 Weirauch, M. T., Barski, A., & Namekawa, S. H. (2020). Super-enhancer switching
619 drives a burst in gene expression at the mitosis-to-meiosis transition. *Nat Struct Mol Biol*,
620 *27*(10), 978-988. https://doi.org/10.1038/s41594-020-0488-3
621 Maezawa, S., Yukawa, M., Alavattam, K. G., Barski, A., & Namekawa, S. H. (2018). Dynamic
622 reorganization of open chromatin underlies diverse transcriptomes during
623 spermatogenesis. *Nucleic Acids Res*, *46*(2), 593-608. https://doi.org/10.1093/nar/gkx1052
624 Meyer, L. R., Zweig, A. S., Hinrichs, A. S., Karolchik, D., Kuhn, R. M., Wong, M., Sloan, C. A.,
625 Rosenbloom, K. R., Roe, G., Rhead, B., Raney, B. J., Pohl, A., Malladi, V. S., Li, C. H.,
626 Lee, B. T., Learned, K., Kirkup, V., Hsu, F., Heitner, S., . . . Kent, W. J. (2013). The
627 UCSC Genome Browser database: extensions and updates 2013. *Nucleic Acids Res*,
628 *41*(Database issue), D64-69. https://doi.org/10.1093/nar/gks1048
629 Nair, S. S., Coolen, M. W., Stirzaker, C., Song, J. Z., Statham, A. L., Strbenac, D., Robinson, M.
630 D., & Clark, S. J. (2011). Comparison of methyl-DNA immunoprecipitation (MeDIP) and
631 methyl-CpG binding domain (MBD) protein capture for genome-wide DNA methylation
632 analysis reveal CpG sequence coverage bias. *Epigenetics*, *6*(1), 34-44.
633 https://doi.org/10.4161/epi.6.1.13313
634 Oakes, C. C., La Salle, S., Smiraglia, D. J., Robaire, B., & Trasler, J. M. (2007). A unique
635 configuration of genome-wide DNA methylation patterns in the testis. *Proc Natl Acad Sci*
636 *U S A*, *104*(1), 228-233. https://doi.org/10.1073/pnas.0607521104
637 Prasasya, R. D., Caldwell, B. A., Liu, Z., Wu, S., Leu, N. A., Fowler, J. M., Cincotta, S. A., Laird,
638 D. J., Kohli, R. M., & Bartolomei, M. S. (2024). Iterative oxidation by TET1 is required
639 for reprogramming of imprinting control regions and patterning of mouse sperm
640 hypomethylated regions. *Dev Cell*. https://doi.org/10.1016/j.devcel.2024.02.012
641 Sachs, M., Onodera, C., Blaschke, K., Ebata, K. T., Song, J. S., & Ramalho-Santos, M. (2013).
642 Bivalent chromatin marks developmental regulatory genes in the mouse embryonic
643 germline in vivo. *Cell Rep*, *3*(6), 1777-1784. https://doi.org/10.1016/j.celrep.2013.04.032
644 Sakashita, A., Ooga, M., Otsuka, K., Maezawa, S., Takeuchi, C., Wakayama, S., Wakayama, T., &
645 Namekawa, S. H. (2023). Polycomb protein SCML2 mediates paternal epigenetic
646 inheritance through sperm chromatin. *Nucleic Acids Res*, *51*(13), 6668-6683.
647 https://doi.org/10.1093/nar/gkad479
648 Sasaki, H., & Matsui, Y. (2008). Epigenetic events in mammalian germ-cell development:
649 reprogramming and beyond. *Nat Rev Genet*, *9*(2), 129-140.
650 https://doi.org/10.1038/nrg2295
651 Schaefer, C. B., Ooi, S. K., Bestor, T. H., & Bourc'his, D. (2007). Epigenetic decisions in
652 mammalian germ cells. *Science*, *316*(5823), 398-399.
653 https://doi.org/10.1126/science.1137544
654 Schmidl, C., Rendeiro, A. F., Sheffield, N. C., & Bock, C. (2015). ChIPmentation: fast, robust,
655 low-input ChIP-seq for histones and transcription factors. *Nat Methods*, *12*(10), 963-965.
656 https://doi.org/10.1038/nmeth.3542
657 Schneider, C. A., Rasband, W. S., & Eliceiri, K. W. (2012). NIH Image to ImageJ: 25 years of
658 image analysis. *Nat Methods*, *9*(7), 671-675. https://doi.org/10.1038/nmeth.2089

Seisenberger, S., Andrews, S., Krueger, F., Arand, J., Walter, J., Santos, F., Popp, C., Thienpont, B., Dean, W., & Reik, W. (2012). The dynamics of genome-wide DNA methylation reprogramming in mouse primordial germ cells. *Mol Cell*, *48*(6), 849-862. https://doi.org/10.1016/j.molcel.2012.11.001

Shao, Z., Zhang, Y., Yuan, G. C., Orkin, S. H., & Waxman, D. J. (2012). MAnorm: a robust model for quantitative comparison of ChIP-Seq data sets. *Genome Biol*, *13*(3), R16. https://doi.org/10.1186/gb-2012-13-3-r16

Shen, L., Inoue, A., He, J., Liu, Y., Lu, F., & Zhang, Y. (2014). Tet3 and DNA replication mediate demethylation of both the maternal and paternal genomes in mouse zygotes. *Cell Stem Cell*, *15*(4), 459-471. https://doi.org/10.1016/j.stem.2014.09.002

Shirakawa, T., Yaman-Deveci, R., Tomizawa, S., Kamizato, Y., Nakajima, K., Sone, H., Sato, Y., Sharif, J., Yamashita, A., Takada-Horisawa, Y., Yoshida, S., Ura, K., Muto, M., Koseki, H., Suda, T., & Ohbo, K. (2013). An epigenetic switch is crucial for spermatogonia to exit the undifferentiated state toward a Kit-positive identity. *Development*, *140*(17), 3565-3576. https://doi.org/10.1242/dev.094045

Shirane, K., Miura, F., Ito, T., & Lorincz, M. C. (2020). NSD1-deposited H3K36me2 directs de novo methylation in the mouse male germline and counteracts Polycomb-associated silencing. *Nat Genet*, *52*(10), 1088-1098. https://doi.org/10.1038/s41588-020-0689-z

Siebert-Kuss, L. M., Dietrich, V., Di Persio, S., Bhaskaran, J., Stehling, M., Cremers, J. F., Sandmann, S., Varghese, J., Kliesch, S., Schlatt, S., Vaquerizas, J. M., Neuhaus, N., & Laurentino, S. (2024). Genome-wide DNA methylation changes in human spermatogenesis. *Am J Hum Genet*, *111*(6), 1125-1139. https://doi.org/10.1016/j.ajhg.2024.04.017

Siklenka, K., Erkek, S., Godmann, M., Lambrot, R., McGraw, S., Lafleur, C., Cohen, T., Xia, J., Suderman, M., Hallett, M., Trasler, J., Peters, A. H., & Kimmins, S. (2015). Disruption of histone methylation in developing sperm impairs offspring health transgenerationally. *Science*, *350*(6261), aab2006. https://doi.org/10.1126/science.aab2006

Sin, H. S., Kartashov, A. V., Hasegawa, K., Barski, A., & Namekawa, S. H. (2015). Poised chromatin and bivalent domains facilitate the mitosis-to-meiosis transition in the male germline. *BMC Biol*, *13*, 53. https://doi.org/10.1186/s12915-015-0159-8

Wang, L., Zhang, J., Duan, J., Gao, X., Zhu, W., Lu, X., Yang, L., Zhang, J., Li, G., Ci, W., Li, W., Zhou, Q., Aluru, N., Tang, F., He, C., Huang, X., & Liu, J. (2014). Programming and inheritance of parental DNA methylomes in mammals. *Cell*, *157*(4), 979-991. https://doi.org/10.1016/j.cell.2014.04.017

Weber, M., Hellmann, I., Stadler, M. B., Ramos, L., Pääbo, S., Rebhan, M., & Schübeler, D. (2007). Distribution, silencing potential and evolutionary impact of promoter DNA methylation in the human genome. *Nat Genet*, *39*(4), 457-466. https://doi.org/10.1038/ng1990

Yamaguchi, K., Hada, M., Fukuda, Y., Inoue, E., Makino, Y., Katou, Y., Shirahige, K., & Okada, Y. (2018). Re-evaluating the Localization of Sperm-Retained Histones Revealed the Modification-Dependent Accumulation in Specific Genome Regions. *Cell Rep*, *23*(13), 3920-3932. https://doi.org/10.1016/j.celrep.2018.05.094

Yin, Q., Yang, C. H., Strelkova, O. S., Wu, J., Sun, Y., Gopalan, S., Yang, L., Dekker, J., Fazzio, T. G., Li, X. Z., Gibcus, J., & Rando, O. J. (2023). Revisiting chromatin packaging in mouse sperm. *Genome Res*, *33*(12), 2079-2093. https://doi.org/10.1101/gr.277845.123

Yoshida, K., Muratani, M., Araki, H., Miura, F., Suzuki, T., Dohmae, N., Katou, Y., Shirahige, K., Ito, T., & Ishii, S. (2018). Mapping of histone-binding sites in histone replacement-completed spermatozoa. *Nat Commun*, *9*(1), 3885. https://doi.org/10.1038/s41467-018-06243-9

Zhang, Y., Liu, T., Meyer, C. A., Eeckhoute, J., Johnson, D. S., Bernstein, B. E., Nusbaum, C., Myers, R. M., Brown, M., Li, W., & Liu, X. S. (2008). Model-based analysis of ChIP-Seq (MACS). *Genome Biol*, *9*(9), R137. https://doi.org/10.1186/gb-2008-9-9-r137

Zheng, H., Huang, B., Zhang, B., Xiang, Y., Du, Z., Xu, Q., Li, Y., Wang, Q., Ma, J., Peng, X., Xu, F., & Xie, W. (2016). Resetting Epigenetic Memory by Reprogramming of Histone Modifications in Mammals. *Mol Cell*, *63*(6), 1066-1079. https://doi.org/10.1016/j.molcel.2016.08.032

Figure legends

Figure 1: Global characteristics of DNA methylation during spermatogenesis.

(A) Schematic of spermatogenesis and the four representative stages analyzed in this study (THY1$^+$, KIT$^+$, PS, and RS). The time window of the transient reduction of DNA methylation is indicated.

(B) ELISA-based quantification of 5-mC during spermatogenesis. Percentage of 5mC in total DNA is shown.

(C, D) Immunostaining of paraffin sections of adult testes with anti-5mC antibody and antibodies against stage-specific markers (ZBTB16 and H1T). Slides were counterstained with DAPI. Images were acquired with a confocal microscope. Regions bordered by dashed yellow squares are magnified in the right panels. Scale bar in the left panel: 20 μm; scale bar in the right panel: 5 μm.

Figure 2: MethylCap-seq analysis during spermatogenesis.

(A) Dynamic changes in DNA methylation during spermatogenesis. MAnorm analysis of MethylCap-seq at each transition of spermatogenesis. The genomic distribution of each peak is shown with colored bars.

(B) Track view of MethylCap-seq data of a representative genomic region for each stage of spermatogenesis. Two biological replicates are shown. Sites with loss of DNA methylation are underlaid in green and indicated by green arrows; sites with gain of DNA methylation are underlaid in red and indicated by red arrows.

(C) Average tag density plots of MethylCap-seq reads in each representative group of genes defined in a previous study (Sin et al., 2015).

Figure 3: Changes in DNA methylation during spermatogenesis.

(A) Enrichment analysis of MethylCap-seq around TSSs (±2 kb) at each transition during spermatogenesis. Pearson correlation values are shown.

(B) Volcano plots for the enrichment and P-values of distal MethylCap-seq outside ±1 kb of TSSs during the transition from KIT$^+$ spermatogonia to PS. Peaks were detected by MAnorm.

(C) GO enrichment analyses for 909 genes losing 5mC and 753 genes gaining 5mC from KIT$^+$ spermatogonia to PS.

(D) RNA-seq heatmap for 909 genes losing 5mC from KIT$^+$ spermatogonia to PS.

(E) Pie charts showing gene expression changes in three groups of genes (909 genes losing 5mC, 753 genes gaining 5mC, and all genes).

Figure 4: Sites of DNA demethylation preset sites of nucleosome retention during spermatogenesis.

(A) Box-and-whisker plots showing mononucleosome enrichment at each genomic locus for each class of genes. Central bars represent medians, the boxes encompass 50% of the data points, and the whiskers indicate 90% of the data points. * P-value < 0.0001, Mann–Whitney U test.
(B) Genomic distribution of mononucleosome peaks in sperm (total 36,911 peaks): MNase-seq data (Erkek et al., 2013). Peaks are detected by MACS2 (Padj-value<0.01, Fold enrichment>5).
(C, D) Changes in the enrichment of H3K4me3 (X-axis) and mononucleosomes in spermatozoa (Y-axes) at demethylated promoters (C) and exons (D) at the mitosis-to-meiosis transition.

Figure 5: Sites of DNA demethylation preset sites of bivalent genomic domains in spermatozoa.

(A) Mononucleosome enrichment in spermatozoa at genomic sites of MethylCap-seq peaks of KIT^+ spermatogonia. Class I (green): genomic sites that are demethylated at the mitosis-to-meiosis transition, and Class II (red): all other sites.
(B) H3.3 enrichment in the two classes of genomic sites in sperm.
(C) Enrichment of H3.3 and nucleosomes
(D) Enrichment of SCML2 in cultured germline stem (GS) cells, and H3.3 enrichment in sperm (left) and mononucleosome enrichment in sperm (right)
(E) Enrichment of H3K27me3 and H3K4me3 during spermatogenesis and in spermatozoa.
(F) RNA-seq analysis in embryos for three groups of genes. Top 1,000 nucleosome-enriched genes among class I and II peak-containing genes at promoters (7,577 and 7,261 genes) and bottom 3,000 nucleosome-enriched genes (Nucleosome-depleted genes).

Figure 6: Model: Sites of DNA demethylation preset sites of nucleosome retention during spermatogenesis.

Genomic regions that are demethylated during the transition from mitotic spermatogonia to meiotic spermatocytes acquire H3K4me3 in meiotic spermatocytes, leading to SCML2-mediated deposition of H3K27me3, thereby establishing persisting bivalent marks at these hypomethylated nucleosome retention sites in spermatozoa.

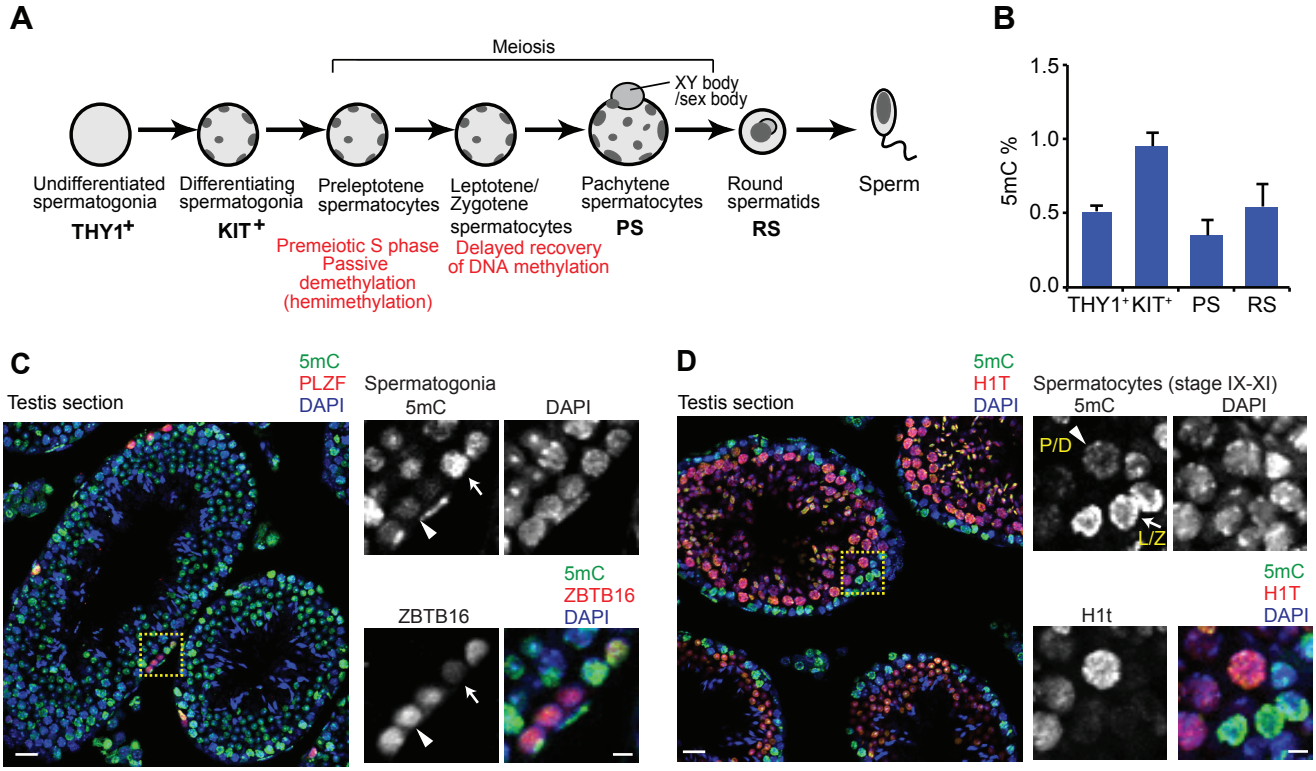

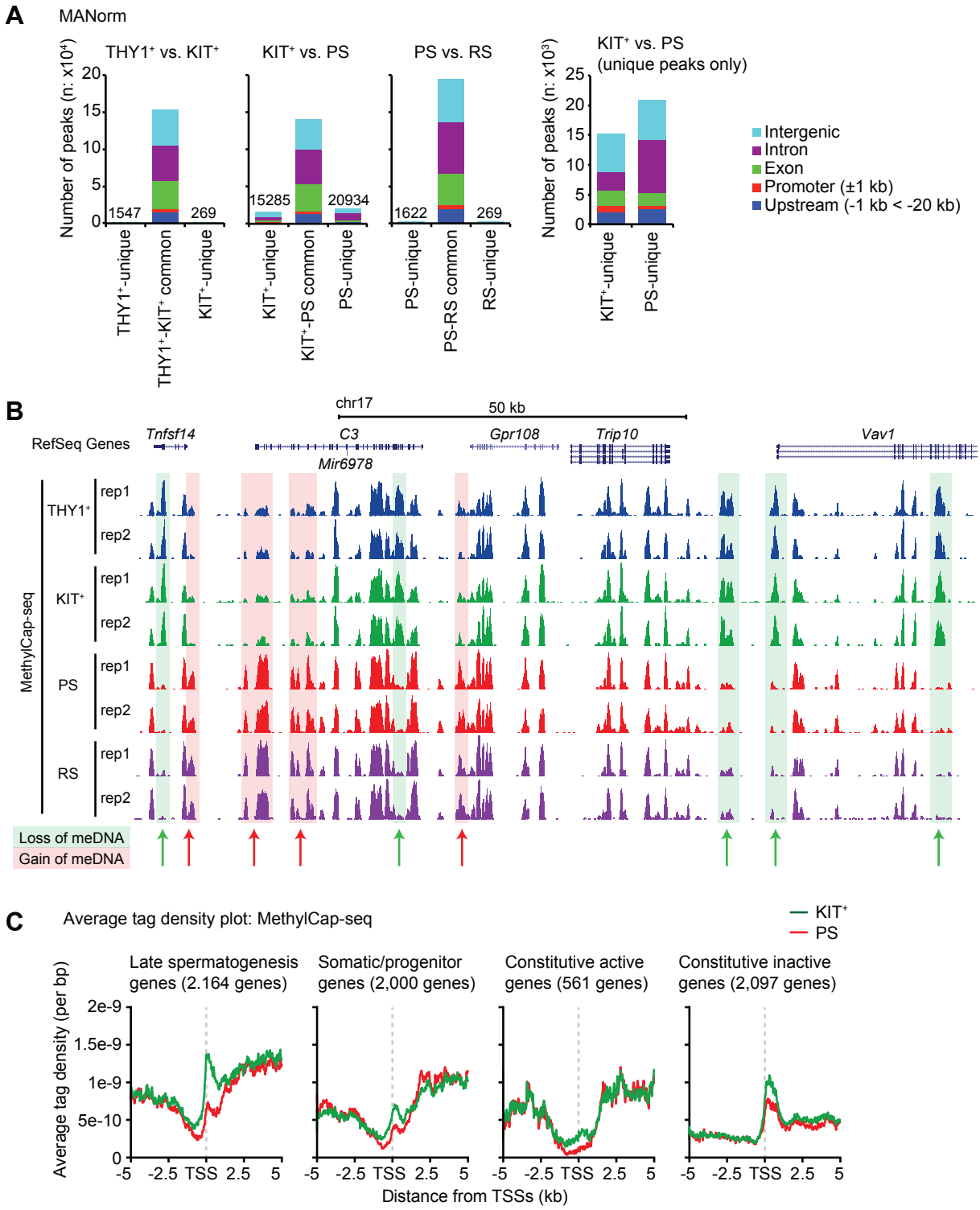

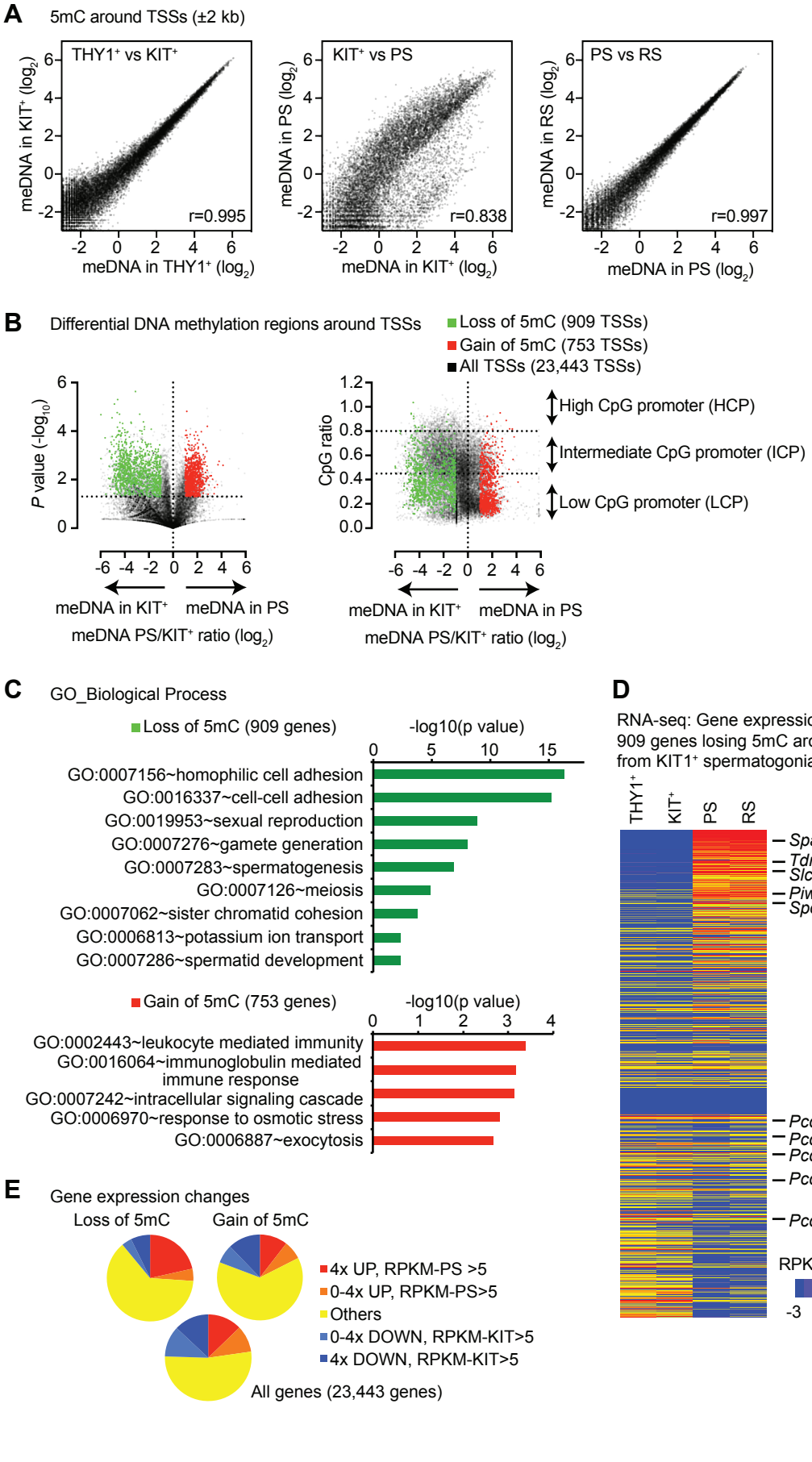

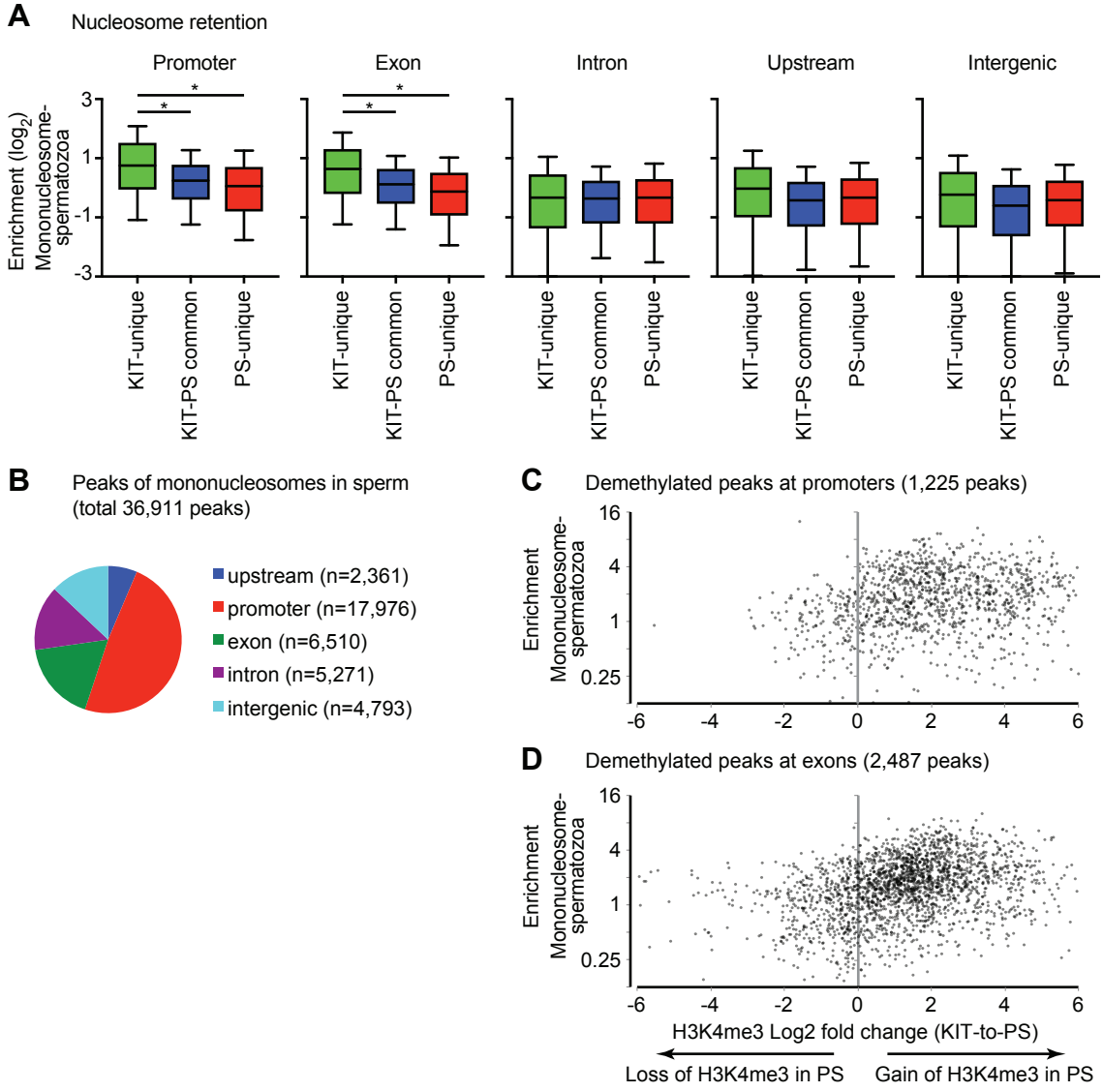

Maezawa et al. Figure 5

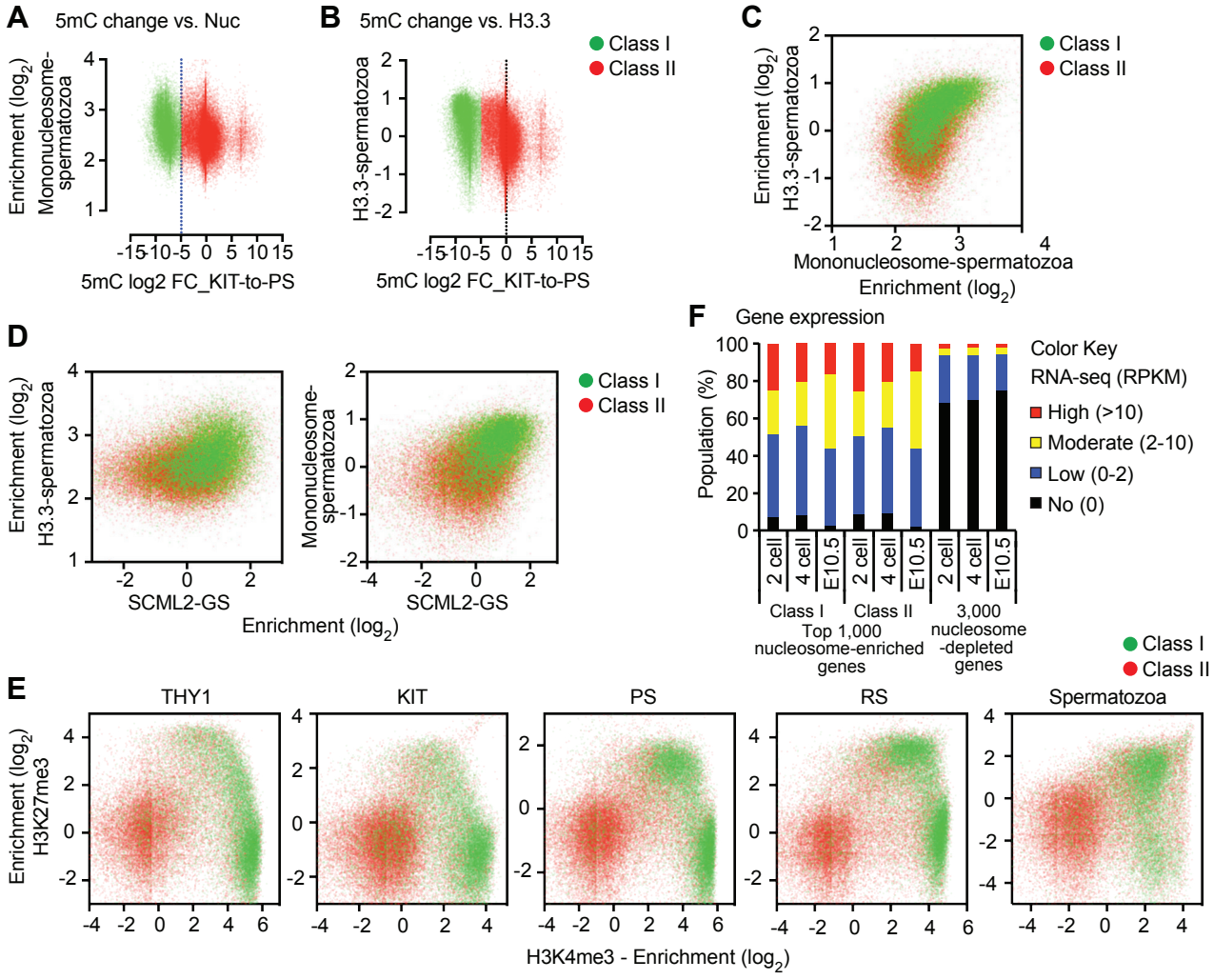

Maezawa et al. Figure 6